A 3D modeling method of layered acoustic material structures with finite dimensions

Gergely Firtha[1,2]
ENTEL Engineering Research & Consulting Ltd. Inspired Acoustics division
Szépvölgyi út 32., H-1025 Budapest, Hungary;

Department of Networked Systems and Services, Faculty of Electric Engineering, Budapest
University of Technology and Economics, Műegyetem rkp. 3., H-1111 Budapest, Hungary

Csaba Huszty[3]
ENTEL Engineering Research & Consulting Ltd. Inspired Acoustics division
Szépvölgyi út 32., H-1025 Budapest, Hungary

ABSTRACT

Modeling of layered acoustic structures to predict the sound absorption characteristics of complex materials is a widely used method in room acoustic practice. Commonly used modeling techniques—such as the transfer matrix method—typically assume locally reacting surfaces of infinite lateral dimensions and provide one-dimensional calculations only, offering limited accuracy, especially for resonant absorbers with finite dimensions. We present the direct, analytical modeling of sound propagation in extendedly reacting layered materials of finite dimensions allowing the estimation of the surface impedance or admittance distribution of layered structures, from which sound absorption properties can be calculated. The theoretical results are validated by measurements, performed on a small-sized resonant panel absorber. We present the implementation of the method in the soundy.ai application.

1. INTRODUCTION

The analytical and numerical modeling of sound absorber structures has been the subject of extensive research over the last decades [8].

As most absorbers are consist of multiple layers of different materials, the basic task of modaling can be summarized as characterizing mechanical wave propagation in the individual layers and the coupling the layers. Once the acoustic behaviour at the top of the structure is known, the absorption characteristics of the ensemble can be predicted when exposed to an incident wave field. Commonly used absorber structures use air gaps, cavities, and limp, or perforated plates with various properties to control the frequency range of absorption, while porous materials inside the structure provide energy dissipation.

The automatition of the coupling of the layers is only possible for highly simplified problem geometries, such as the transfer matrix method (TMM) [3], which assumes planar layers of infinite
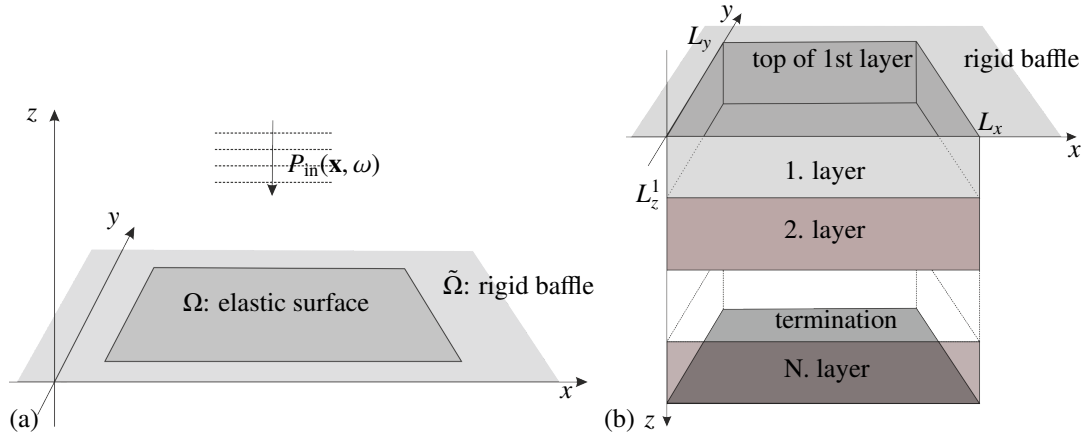

Figure 1: Geometry for scattering from an elastic surface (a) and the layered absorber structure under discussion (b)

lateral size exposed to plane waves. Furthermore, it is assumed that the layers are locally reactive, i.e. lateral wave propagation inside the layers is not considered. Although a simple radiation efficiency-based size correction can be included in the TMM method, the potential lateral modal behavior of finite-sized absorbers cannot be accounted for [3].

In this paper, we propose an analytical modeling method for the 3D modeling of layered absorber structures. Our method relies on expressing the two-dimensional input impedance function/matrix of each layer as a function of the bottom impedance, i.e., the input impedance of the previous layer. Once the surface impedance/admittance of the top layer is expressed, the scattered field can be calculated at the surface for an arbitrary incident wave field, allowing for the formulation of the absorption coefficient of the total structure. We compare the results of our analytical model with an actual plate resonator, which consists of a limp membrane, an air cavity, and a porous layer. We verify that once the material parameters of the model are chosen in accordance with the actual structure, our proposed model provides a qualitatively fair approximation for the involved physical processes.

2. METHODOLOGY FOR MODELING LAYERED STRUCTURES

In order to predict the absorption characteristics of an arbitrary, finite absorbing surface the correspond scattering problem has to be solved for an arbitrary incident sound. This section introduces how the involved scattering problem can be solved in a planar geometry once the surface admittance function is known over the top layer of the potentially layered absorber structure. Once the total pressure field is known along the elastic surface the absorbtion coefficient can be evaluted, inherently including finite-size effects (e.g. diffraction at the edge of the absorber). The derivation follows as given in [?]

2.1. Calculating scattering from baffled elastic surface

In the present paper exclusively planar geometries are investigated. Consider a two-dimensional, bounded elastic surface with finite dimensions, baffled into a infinite rigid plane located at $z = 0$. The geometry under investigation is illustrated in Figure 1 (a) through a rectangular plate as a representative example. The region over the elastic surface is referred to as Ω, whereas the points situated on the rigid plane are denoted by $\tilde{\Omega}$.

The plane is loaded by the infinite half-space of fluid with the density of ρ_0 and in which the speed of sound is denoted by c. An arbitrary steady state incident wave field $P_{in}(\mathbf{x}, \omega)$ is propagating towards the elastic plate, oscillating at an angular frequency ω.

As the incident wave interacts with the surface the total pressure field can be written above and

on the surface as

$$P_{\text{tot}}(\mathbf{x}, \omega) = P_{\text{in}}(\mathbf{x}, \omega) + \underbrace{P_{\text{refl}}(\mathbf{x}, \omega) + P_{\text{rerad}}(\mathbf{x}, \omega)}_{P_{\text{scat}}(\mathbf{x}, \omega)}. \tag{1}$$

The scattered field (denoted by $P_{\text{scat}}(\mathbf{x}, \omega)$) is composed of two components: a part of the incident field is directly reflected from the surface (denoted as $P_{\text{refl}}(\mathbf{x}, \omega)$), and a reradiated component ($P_{\text{rerad}}(\mathbf{x}, \omega)$). The latter is generated by the vibrating elastic surface, which is in motion due to the force distribution arising from the total pressure field.

The current problem geometry has the following boundary conditions:

– The total velocity on the infinite rigid baffle is zero, which results in:

$$\frac{\partial}{\partial z} P_{\text{in}}(\mathbf{x}, \omega) = -\frac{\partial}{\partial z} P_{\text{scat}}(\mathbf{x}, \omega) \tag{2}$$

$$P_{\text{in}}(\mathbf{x}, \omega) = P_{\text{scat}}(\mathbf{x}, \omega), \quad \mathbf{x} \in \tilde{\Omega} \tag{3}$$

– The elastic surface has an admittance function (including self and mutual admittances) defined between each point, expressed as:

$$Y_{\text{surf}}(\mathbf{x}, \mathbf{x}_0, \omega) = \frac{A(\mathbf{x}, \omega)}{P(\mathbf{x}_0, \omega)}, \tag{4}$$

where $A(\mathbf{x}, \omega)$ represents the normal acceleration of the surface at the receiver position $\mathbf{x}$, and $P(\mathbf{x}_0)$ is the pressure at the source position $\mathbf{x}_0$. Assuming a continuous pressure distribution along the elastic surface, the corresponding acceleration can be obtained as the convolutional integral

$$A(\mathbf{x}, \omega) = \int_{\Omega} Y_{\text{surf}}(\mathbf{x}, \mathbf{x}_0, \omega) P(\mathbf{x}_0, \omega) \, d\mathbf{x}_0. \tag{5}$$

Since the scattered field propagates merely towards the positive half space it can be written in terms of a Rayleigh integral along $z = 0$ [1,2], yielding the expression for the total field at an arbitrary receiver position $\mathbf{x} = [x, \; y, \; z \geq 0]^{\text{T}}$

$$P_{\text{tot}}(\mathbf{x}, \omega) = P_{\text{in}}(\mathbf{x}, \omega) - 2 \int_{\Omega \cup \tilde{\Omega}} \underbrace{\frac{\partial}{\partial z} P_{\text{scat}}(\mathbf{x}_0, \omega)}_{\frac{\partial}{\partial z} P_{\text{scat}}(\mathbf{x}, \omega)|_{\mathbf{x} = \mathbf{x}_0}} G(\mathbf{x}, \mathbf{x}_0, \omega) d\mathbf{x}_0, \tag{6}$$

where

$$G(\mathbf{x}, \mathbf{x}_0, \omega) = \frac{1}{4\pi} \frac{e^{-j\frac{\omega}{c}|\mathbf{x} - \mathbf{x}_0|}}{|\mathbf{x} - \mathbf{x}_0|} \tag{7}$$

being the 3D Green's function, describing the field of a point source located at $\mathbf{x}_0$, measured at $\mathbf{x}$.

By substuting $P_{\text{scat}} = P_{\text{tot}} - P_{\text{in}}$ the integral can be factorized as

$$P_{\text{tot}}(\mathbf{x}, \omega) = P_{\text{in}}(\mathbf{x}, \omega) - 2 \int_{\Omega} \frac{\partial}{\partial z} P_{\text{tot}}(\mathbf{x}_0, \omega) G(\mathbf{x}, \mathbf{x}_0, \omega) d\mathbf{x}_0 -$$

$$-2 \underbrace{\int_{\tilde{\Omega}} \frac{\partial}{\partial z} P_{\text{tot}}(\mathbf{x}_0, \omega) G(\mathbf{x}, \mathbf{x}_0, \omega) d\mathbf{x}_0}_{0} + 2 \underbrace{\int_{\Omega \cup \tilde{\Omega}} \frac{\partial}{\partial z} P_{\text{in}}(\mathbf{x}_0, \omega) G(\mathbf{x}, \mathbf{x}_0, \omega) d\mathbf{x}_0}_{P_{\text{refl}}^{\text{rigid}}(\mathbf{x})}. \tag{8}$$

Here it was utilized that the middle integral term vanishes over the rigid baffle, while the rightmost integral describes the reflected field from an ideally rigid infinite plane (i.e. as the elastic surface was not present). The pressure gradient in the air is expressed by the Euler's relation $\frac{\partial}{\partial z} P(\mathbf{x}, \omega) = -\rho_0 A(\mathbf{x})$,

and the radiation problem in air can be coupled with the surface motion by the boundary condition Equation 5, leading finally to

$$P_{\text{tot}}(\mathbf{x}, \omega) = P_{\text{in}}(\mathbf{x}, \omega) + P_{\text{refl}}^{\text{rigid}}(\mathbf{x}, \omega) + 2\rho_0 \int_\Omega \left(\int_\Omega Y_{\text{surf}}(\mathbf{x}_0, \mathbf{x}_1, \omega) P_{\text{tot}}(\mathbf{x}_1, \omega)\, \mathrm{d}\mathbf{x}_1 \right) G(\mathbf{x}, \mathbf{x}_0, \omega)\mathrm{d}\mathbf{x}_0. \quad (9)$$

The equation describes the total field at an arbitrary receiver position $\mathbf{x}$ above the horizontal plane implicitly. Finally, restricting the receiver position to the elastic surface the above expression simplifies to

$$P_{\text{tot}}(\mathbf{x}, \omega) = 2P_{\text{in}}(\mathbf{x}, \omega) + 2\rho_0 \int_\Omega \left(\int_\Omega Y_{\text{surf}}(\mathbf{x}_0, \mathbf{x}_1, \omega) P_{\text{tot}}(\mathbf{x}_1, \omega)\, \mathrm{d}\mathbf{x}_1 \right) G(\mathbf{x}, \mathbf{x}_0, \omega)\mathrm{d}\mathbf{x}_0, \quad (10)$$

with $\mathbf{x} = [x,\ y,\ 0]^{\text{T}}$, while the total normal velocity of the surface can be calculated as

$$V_{\text{tot}}(\mathbf{x}, \omega) = \frac{1}{\mathrm{j}\omega} \int_\Omega Y_{\text{surf}}(\mathbf{x}, \mathbf{x}_0, \omega) P_{\text{tot}}(\mathbf{x}_0, \omega)\, \mathrm{d}\mathbf{x}_0. \quad (11)$$

The equation Equation 10 presents the total pressure field as an integral equation, which cannot be solved analytically. However, it can be numerically solved by discretizing the elastic surface into I elements, with the center of each element $\mathbf{x}_i$ and area $\mathrm{d}\Omega_i$. The complex amplitudes of pressure and normal velocity at $\mathbf{x}_i$ are given by the vectors $\mathbf{p} = P_i = P(\mathbf{x}_i)$ and $\mathbf{a} = A_i = A(\mathbf{x}_i)$, and their interconnection is described by the admittance matrix

$$\mathbf{Y}_{\text{surf}} = Y_{ij} = \frac{A_i}{P_j}. \quad (12)$$

By introducing the Green's matrix on the surface

$$\mathbf{G} = G_{ij} = \int_{\mathrm{d}\Omega_i} G(\mathbf{x}_j, \mathbf{x}_0)\mathrm{d}\mathbf{x}_0, \quad \mathbf{x}_j = [x,\ y,\ z = 0]^{\text{T}} \quad (13)$$

and discretizing equation Equation 10, we obtain

$$\mathbf{p}_{\text{tot}} = 2\mathbf{p}_{\text{in}} + 2\rho_0 \mathbf{G}\,\mathbf{Y}_{\text{surf}}\,\mathbf{p}_{\text{tot}}. \quad (14)$$

The total field on the surface of the plate is obtained by solving the system of equations using

$$\mathbf{p}_{\text{tot}} = 2\,(\mathbf{I} - 2\rho_0\mathbf{G}\mathbf{Y}_{\text{surf}})^{-1}\,\mathbf{p}_{\text{in}}. \quad (15)$$

and the corresponding normal velocity distribution from the discrete form of equation Equation 11 as

$$\mathbf{v}_{\text{tot}} = \frac{1}{\mathrm{j}\omega}\mathbf{Y}_{\text{surf}}\mathbf{p}_{\text{tot}}. \quad (16)$$

2.2. Definition of absorption coefficient for extended reactive surfaces

Having found the total pressure field and velocity distribution on the surface of the absorber for an arbitrary incident wave, its absorption characteristics can be predicted as follows: The incident field is assumed to be a plane wave arriving to the elastic surface at an elevation angle of θ and azimuth angle of ϕ, described by

$$P_{\text{in}}(\mathbf{x}, \theta, \phi, \omega) = \mathrm{e}^{-\mathrm{j}k(\cos\phi\sin\theta x + \sin\phi\sin\theta y + \cos\theta z)}. \quad (17)$$

As a straightforward estimation, the directional absorption coefficient of the elastic surface can be defined as (see eq. (12.30) [3])

$$\alpha(\theta, \phi, \omega) = \frac{\Pi_{\text{abs}}(\theta, \phi, \omega)}{\Pi_{\text{in}}(\theta, \omega)} = Z_0 \frac{\mathrm{Re}\left(\int_\Omega P_{\text{tot}}(\mathbf{x}, \theta, \phi, \omega) V_{\text{tot}}^*(\mathbf{x}, \theta, \phi, \omega)\, \mathrm{d}\mathbf{x} \right)}{\cos\theta\, S_\Omega}, \quad (18)$$

with Π_{abs} and Π_{in} being the absorbed and incident power, S_Ω being the area of the elastic surface and $Z_0 = \rho_c c$ being the specific impedance of air. In the discrete case the absorbed power can be written as

$$\Pi_{\text{abs}}(\theta, \phi, \omega) = \text{Re}\left((\mathbf{p}_{\text{tot}}^* \mathbf{v}_{\text{tot}})^*\right) = \text{Re}\left(\left(\frac{1}{j\omega}\mathbf{p}_{\text{tot}}^* \mathbf{Y}\mathbf{p}_{\text{tot}}\right)^*\right) = -\frac{1}{\omega}\text{Im}\left(\mathbf{p}_{\text{in}}^* \mathbf{T}^* \mathbf{Y}_{\text{surf}} \mathbf{T}\mathbf{p}_{\text{in}}\right) \tag{19}$$

with denoting $\mathbf{T} = 2\left(\mathbf{I} - 2\rho_0 \mathbf{G}\mathbf{Y}_{\text{surf}}\right)^{-1}$.

The diffuse field absorption coefficient is calculated by averaging the absorbed and incident power over the possible incident directions, resulting in

$$\alpha^{\text{diff}} = \frac{\int_0^{2\pi} \int_0^{\pi/2} \Pi_{\text{abs}}(\theta, \phi) \sin\theta \mathrm{d}\theta\, \mathrm{d}\phi}{\int_0^{2\pi} \int_0^{\pi/2} \Pi_{\text{in}}(\theta) \sin\theta \mathrm{d}\theta\, \mathrm{d}\phi} = Z_0 \frac{\int_0^{2\pi} \int_0^{\pi/2} \Pi_{\text{abs}}(\theta, \phi) \sin\theta \mathrm{d}\theta\, \mathrm{d}\phi}{\pi S_\Omega}. \tag{20}$$

2.3. Coupling the layered structure

The previous section highlighted that once the admittance function (or admittance matrix in the discrete case) is known over a finite elastic surface the scattering problem can be solved numerically for an arbitrary incident field. From the resulting total pressure field the and surface velocity the absorption properties of the surface can be evaluated.

In the following it is assumed the elastic surface is the top of a layered absorber structure, consisting of multiple fluid (air) layers, porous absorbing layers or thin plate layers. Our goal is to express the surface admittance of the top layer, so that absorption properties can be predicted numerically from it. In the following it is discussed how the layers can be coupled to each other by surface impedance/admittance boundary conditions with solving the equation of motion in each layer analytically, eventually allowing the expression of the top layer's surface admittance. The method is, therefore, a 3-dimensional extension of the 1-dimensional transfer matrix method, applied frequently the prediction of the absorption proerties of layered structures with infinite lateral extension, by coupling the individual layers through locally reactive impedances.

The geometry of the layered structure is depicted in Figure 1 (b). The layers under investigation have a rectangular cross-section with horizontal dimensions of L_x and L_y. The lateral sides of the layers are assumed to be completely rigid, meaning that rigid boundary conditions are prescribed. However, other absorber shapes and lateral boundary conditions can be implemented straightwardly by finding a corresponding set of modal basis functions, discussed inthe following subsection.

The methodology for coupling the layers is as follows: It is assumed that the impedance can be expressed at the top of the n-th layer as the function of the impedance measured at the bottom of the layered. The impedance at the top of the n. layer is defined as

$$Z_{\text{top}}^n(\mathbf{x}, \mathbf{x}_0, \omega, Z_{\text{bottom}}^n = Z_{\text{top}}^{n+1}) = \frac{P(\mathbf{x}, \omega)}{A(\mathbf{x}_0, \omega)} \tag{21}$$

i.e. describes the pressure field at $\mathbf{x} = [x, y]^{\text{T}}$ due to a acceleration excitation at $\mathbf{x}_0 = [x_0, y_0]^{\text{T}}$. The impedance at the bottom of the n-th layer equals the top impedance of the $(n-1)$-th layer as a continuity condition. Starting from the lowermost layer, which is terminated by $Z_{\text{t}}(\mathbf{x}, \omega)$, the input surface impedance of the top layer can be written as

$$Z_{\text{surf}}(\mathbf{x}, \mathbf{x}_0, \omega) = Z_{\text{top}}^1(Z_{\text{top}}^2(...Z_{\text{top}}^N(Z_{\text{term}}(\mathbf{x}, \omega)))). \tag{22}$$

The impedance function is evaluated numerically at the top of each layer using the discretization scheme outlined in the previous section. Once the impedance matrix $\mathbf{Z}_{\text{top}}^1$ is obtained at the top layer, the surface admittance matrix is computed as $\mathbf{Y}_{\text{surf}} = (\mathbf{Z}_{\text{top}}^1)^{-1}$, allowing the solution of the scattering problem from the layered structure.

The surface impedance for fluid, porous absorber, and thin panel layers is described next, under the assumption of arbitrary impedance boundary condition at the bottom of the layers.

2.4. Calculation of transfer admittance for a fluid layer

First a rectangular fluid layer is investigated with the horizontal dimensions L_x, L_y, and the vertical thickness of L_z. For the sake of simplicity the top of the layer is located at $z = 0$, thus the bottom of the layer is at $z = L_z$. The equation of motion in the layer is given by the linear 3D wave equation, written in the frequency domain as

$$\left(\nabla_{\mathbf{x}}^2 + \left(\frac{\omega}{c}\right)^2\right) P(\mathbf{x}, \omega) = 0, \tag{23}$$

with $\nabla_{\mathbf{x}}$ denoting the Laplace operator. The input surface impedance is defined directly as being equal to the pressure field at the top of the layer $P(x, y, 0, \omega)$, assuming a point like excitation in the acceleration field, i.e.

$$A(x, y, 0, \omega) = -\rho_0 \frac{\partial}{\partial z} P(x, y, z = 0, \omega) = \delta(\mathbf{x} - \mathbf{x}_0) \quad \rightarrow \quad Z_{\text{top}}(\mathbf{x}, \mathbf{x}_0, \omega) = P(x, y, 0, \omega) \tag{24}$$

The bottom of the layer is terminated by an abitrary impedance distribution Z_{bottom}, written in terms of acceleration

$$P(x, y, L_z) = \iint_0^{L_x, L_y} Z_{\text{bottom}}(x, x_0, y, y_0) A(x_0, y_0, L_z) \, \mathrm{d}x_0 \, \mathrm{d}y_0 \tag{25}$$

With the present lateral boundary conditions all the involved quantites (pressure, acceleration, impedances) can be expanded into the linear combination of horizontal modal basis functions

$$P(x, y, z, \omega) = \sum_{\mathbf{m}} \underbrace{\Phi_m(x) \cdot \Phi_n(y)}_{\Phi_{\mathbf{m}}(\mathbf{x})} \left(p_{\mathbf{m}}^+ e^{-\mathrm{j}k_z^{\mathbf{m}} z} + p_{\mathbf{m}}^- e^{\mathrm{j}k_z^{\mathbf{m}} z}\right) \tag{26}$$

with using linear indexing $\mathbf{m} = [m, n]^{\mathrm{T}}$ and $k_z^{\mathbf{m}} = \sqrt{\left(\frac{\omega}{c}\right)^2 - \left(\frac{m\pi}{L_x}\right)^2 - \left(\frac{n\pi}{L_y}\right)^2}$ denoting the z-component of the wavenumber. In Equation 26 $p_{\mathbf{m}}^+$ and $p_{\mathbf{m}}^-$ denote the complex amplitude of plane waves propagating downward and upward in the layer, for which the system of equations has to be solved numerically.

In the present geometry, the modal basis functions, forming a complete, orthonormal basis are given by

$$\Phi_m(x) = \begin{cases} \frac{1}{\sqrt{L_x}}, & m = 0 \\ \sqrt{\frac{2}{L_x}} \cos \frac{m\pi}{L_x} x, & m > 0 \end{cases} \qquad \Phi_n(y) = \begin{cases} \frac{1}{\sqrt{L_y}}, & n = 0 \\ \sqrt{\frac{2}{L_y}} \cos \frac{n\pi}{L_y} y, & n > 0 \end{cases} . \tag{27}$$

Note, that all the following results can be extended unchangedly for non-rectangular cross-sections and non-rigid lateral sides as long as orthonormal modal functions can be found.

In the following the actual derivation is not detailed. As a standard approach, using the modal superposition method (discussed e.g. in [2]) the derivation involves the expansion of equations Equation 24 and Equation 25 into the series of modal basis functions, allowing the analytical evaluation of partial differentiation. The system of equations then can be decoupled by projection of the series to the individual mode shapes. In the decoupled, modal domain the system of equations can be solved for p^+ and p^-, and Equation 26 can be evaluated at $z = 0$ to obtain the surface impedance of the layer.

Again, the problem is solved on a discrete grid of I elements on the layer surface. The modal series are truncated up to the M-th order, i.e. $n = m = 0, 1, 2, ..., M$, resulting in $(M + 1)^2$ modal basis vectors. In a discrete matrix-vector notation the modal basis vectors are ordered into the $(M + 1)^2 \times I$ sized modal matrix $\mathbf{\Phi}$, each row containing a mode shape. With this notation the $I \times I$ sized spatial surface impedance matrix is given on a single angular frequency ω by

$$\mathbf{Z}_{\text{top}} = \mathbf{\Phi}^{\mathrm{T}} \tilde{\mathbf{Z}}_{\text{top}} \mathbf{\Phi}, \tag{28}$$

where the modal coordinate matrix of the top impedance is given by [4]

$$\tilde{\mathbf{Z}}_{\text{top}} = \left(\text{diag}(\cos(\tilde{\mathbf{k}}_{\mathbf{z}}L_z)) - \frac{1}{\rho_0}\tilde{\mathbf{Z}}_{\text{bottom}}\,\text{diag}(\tilde{\mathbf{k}}_{\mathbf{z}}\sin(\tilde{\mathbf{k}}_{\mathbf{z}}L_z))\right)^{-1}\left(\tilde{\mathbf{Z}}_{\text{bottom}}\,\text{diag}(e^{j\tilde{\mathbf{k}}_{\mathbf{z}}L_z}) + \rho_0\text{diag}(\frac{e^{j\tilde{\mathbf{k}}_{\mathbf{z}}L_z}}{j\tilde{\mathbf{k}}_{\mathbf{z}}})\right) - \text{diag}(\frac{\rho_0}{j\tilde{\mathbf{k}}_{\mathbf{z}}}), \quad (29)$$

with $\tilde{\mathbf{k}}_{\mathbf{z}} = k_z^{\mathbf{m}}$ and diag() denoting a diagonal matrix constructed from the input vector. Obviously, Equation 29 implicitly contains the modal matrix of the bottom/termination impedance, defined by

$$\tilde{\mathbf{Z}}_{\text{bottom}} = \iint_0^{L_x,L_y}\iint_0^{L_x,L_y} Z_{\text{bottom}}(\mathbf{x}, \mathbf{x}_0, \omega)\,\Phi_{\mathbf{m}}(\mathbf{x}_0)\,\Phi_{\mathbf{p}}(\mathbf{x})\,\mathrm{d}\mathbf{x}\,\mathrm{d}\mathbf{x}_0 = \mathbf{\Phi}\mathbf{Z}_{\text{bottom}}\mathbf{\Phi}^{\mathrm{T}} \quad (30)$$

It should be noted that for a rigid termination, i.e. if $\tilde{\mathbf{Z}}_{\text{bottom}} = \text{diag}(\infty)$, the above expression converges to

$$\tilde{\mathbf{Z}}_{\text{top}}^{\text{rigid}} = -\rho_0\text{diag}(\frac{\cot(\tilde{\mathbf{k}}_{\mathbf{z}}L_z)}{\tilde{\mathbf{k}}_{\mathbf{z}}}). \quad (31)$$

Obviously, Equation 28 and Equation 30 describe a 2-dimensional orthogonal inverse and forward transform, with the 1D transform matrix given by the modal matrix. The linear transform yields the modal spectrum of the involved 2D quantities. In the modal domain the surface impedance can be expressed from the bottom impedance spectrum, followed by the corresponding inverse transform to the spatial domain.

2.5. Calculation of transfer admittance for porous layers

Although there are more complex models available for modeling sound propagation in porous absorbers with a rigid skeleton, such as the Biot model, the present work uses equivalent fluid models to model porous layers. Specifically, the Delany-Bazley [4], Miki [5], Mechel-Grundman [6], and Allard-Champoux [7] models, which provide expressions for the complex fluid density and the complex speed of sound (including attenuation) based on simple material parameters such as flow resistivity, tortuosity, porosity, and characteristic lengths. These models, which are mainly empirical, enable the direct application of Equation 28 for calculating the top surface impedance of a porous layer without any modification.

2.6. Calculation of transfer admittance for a simply supported plate

Finally, as a third possible layer the input impedance function of a thin plate is investigated, backloaded by an arbitrary bottom impedance distribution.

From thin plate theory it is well-known that the equation of motion for an unloaded plate is given for the normal displacement $W(x, y)$ by

$$\left(\nabla_{\mathbf{x}}^4 - k_f^4\right)W(\mathbf{x}) = 0, \quad (32)$$

with $k_f = (\rho_s h\omega^2/D)^{1/4}$ being the bending wavenumber, ρ_s the density of the plate, h is the thickness of the plate and D being the flexural rigidity. It is assumed that the plate is simply supported, i.e. the plate can not move in the z-direction at its edge, but is free to rotate around its support. The plate is again, considered to be a rectangular one with the same dimensions as the other layers, and equation of motion is again, solved in the modal domain. The mode shapes satisfying the present boundary conditions are given by

$$\Phi_m(x) = \begin{cases} \frac{1}{\sqrt{L_x}}, & m = 0 \\ \sqrt{\frac{2}{L_x}}\sin\frac{m\pi}{L_x}x, & m > 0 \end{cases} \qquad \Phi_n(y) = \begin{cases} \frac{1}{\sqrt{L_y}}, & n = 0 \\ \sqrt{\frac{2}{L_y}}\sin\frac{n\pi}{L_y}y, & n > 0 \end{cases} \quad (33)$$

---

[4]In the following matrices and vectors defined in the modal domain are denoted by tilde.

In our present geometry the bottom of the plate is loaded by the top impedance function of the next layer, denoted by $Z_{\text{bottom}}(\mathbf{x}, \mathbf{x}_0)$. This time, due to the nature of the equation of motion the thin plate layer's top admittance is calcualted directly, from which the impedance function can be calculated straightforwardly if required. Similarly to the fluid layer case, the surface admittance of the plate is found by calculating the acceleration at the surface at point $\mathbf{x}$, due to exciting the plate with a point like pressure distribution at $\mathbf{x}_0$. This approach yields the following inhomogenous equation of motion

$$\frac{D}{(\text{j}\omega)^2}\left(\nabla_{\mathbf{x}}^4 - k_f^4\right)A(\mathbf{x}) = \delta(\mathbf{x} - \mathbf{x}_0)\text{d}S - \underbrace{\iint_0^{Lx,Ly} A(\mathbf{x}_1)\,Z_{\text{bottom}}(\mathbf{x}, \mathbf{x}_1)\,\text{d}\mathbf{x}_1}_{P_{\text{bottom}}(\mathbf{x})}, \tag{34}$$

where $P_{\text{bottom}}(\mathbf{x})$ is the fluid loading, acting on the bottom side of the plate, and $\text{d}S$ is the elementary area, converting the point-like force excitation into pressure excitation.

As for the fluid layer, the inhomogenous equation is solved by expanding $A(\mathbf{x})$ in both sides of the equation into the series of the modal basis function, allowing the analytical evaluation of $\nabla_{\mathbf{x}}^4$. This step is followed by projection of both sides of the equation the mode shapes, leading to the decoupled, modal formulation of the equation of motion. This equation can be rearranged to be solved for the acceleration, directly yielding the admittance function at the angular frequency ω of the surface of the thin plate

$$\mathbf{Y}_{\text{top}} = \mathbf{\Phi}^{\text{T}}\underbrace{\left(\text{diag}\left(\frac{m_s}{\omega^2}\left(\omega^2 - \tilde{\omega}^2\right)\right) + \tilde{\mathbf{Z}}_{\text{bottom}}\right)^{-1}\text{d}S}_{\tilde{\mathbf{Y}}_{\text{top}}}\mathbf{\Phi}, \tag{35}$$

with $m_s = \rho_s h$ being the mass of the plate per unit surface area, $\tilde{\mathbf{Z}}_{\text{bottom}} = \mathbf{\Phi}\mathbf{Z}_{\text{bottom}}\mathbf{\Phi}^{\text{T}}$ is again the modal representation of the bottom loading impedance (see Equation 30) and $\tilde{\omega}$ being the in-vacou eigenfrequencies corresponding to the mode shapes.

Assuming an isotrophic plate the vector of eigenfrequencies is given by

$$\tilde{\omega} = \frac{h}{\sqrt{12}}c\left(\left(\frac{m\pi}{L_x}\right)^2 + \left(\frac{n\pi}{L_y}\right)^2\right), \quad c = \sqrt{\frac{E}{\rho_s(1 - \nu^2)}} \tag{36}$$

where c is the traveling speed of bending waves in the plate, E is the Young's modulus and ν is the Poisson ratio. Considering an ortotrophic plate for which the wave traveling speed is different into x and y dimensions the quantites are extended as

$$\tilde{\omega} = \frac{h}{\sqrt{12}}\left(c_x\left(\frac{m\pi}{L_x}\right)^2 + c_y\left(\frac{n\pi}{L_y}\right)^2\right), \quad c_x = \sqrt{\frac{E_x}{\rho_s(1 - \nu_x\nu_y)}}, c_y = \sqrt{\frac{E_y}{\rho_s(1 - \nu_x\nu_y)}}. \tag{37}$$

Obviously, from the surface admittance the surface impedance is defined as

$$\mathbf{Z}_{\text{top}} = \mathbf{\Phi}^{\text{T}}\underbrace{\left(\text{diag}\left(\frac{m_s}{\omega^2}\left(\omega^2 - \tilde{\omega}^2\right)\right) + \tilde{\mathbf{Z}}_{\text{bottom}}\right)\text{d}S}_{\tilde{\mathbf{Z}}_{\text{top}}}\mathbf{\Phi}, \tag{38}$$

i.e. in the modal domain the loading impedance is simply added to the plate's in-vacou impedance distribution.

3. APPLICATION EXAMPLE: MODELING A PLATE RESONATOR

From the three types of layers discussed in the previous section a simple plate absorber consiting of a plate, and airgap and a porous absorber layer, backed with rigid termination. The lowermost layer is the porous layer, backed with a rigid termination. The layer was modeled as an equivalent fluid based on the Allard-Champoux model, i.e. its impedance was calculated based on Equation 31. The
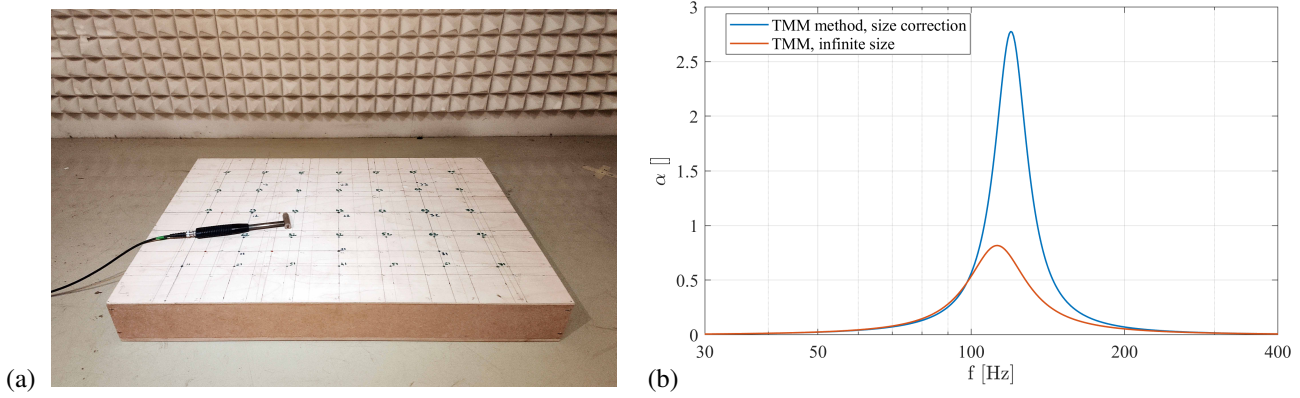
Figure 2: Plate absorber under investigation (a) and the result of TMM modeling (b)

air gap was terminated by the surface impedance of the porous layer, calcualted based on Equation 29. Note that since the modal basis is the same in the two layers, therefore, the 2D inverse and forward transform can be omitted, i.e. Equation 31 can be directly used in Equation 29, coupling the layers in the modal domain. Finally, the top plate's surface impedance is calculated by Equation 38 by utilizing the surface impedance of the air gap, transformed from the fluid's modal basis into that of the plate.

The material parameters of the analytical model was choosen based on an actual, customly built plate resonator structure, allowing the comparison of the model's output with measurements.

3.1. The plate absorber under investigation

Figure 2 (a) shows the customly buit plate resonator. The horizontal dimensions of the structure are $L_x = 88$ cm and $L_y = 62$ cm, which corresponds to a total area of $\Omega = 0.55$ m^2. The absorber is constructed using three layers:

– A 3-layered composite plywood panel with a thickness of $h = 4$ mm, serving as the mass of the resonator structure. In accordance with the manufacturer's datasheet the mass of the plate is approximately $m_s = 2.7$ kg/m^2.

– An air gap of $d_a = 4.3$ cm, together with the air filling the porous absorber layer serving as the spring for the damped mass-spring absorber structure.

– A layer of rock wool with a thickness of $d_p = 5$ cm attached to the back of the structure to ensure energy dissipation in the resonator. The porous absorbing layer's flow resistivity was assumed to be $\sigma_s = 45000$ rayl/m following the manufacturer's datasheet.

The backing and framing of the structure are made of plywood with a thickness of 1.2 cm. In our model the backing and framing was considered to be ideally rigid.

Based on a simple mass-spring system theory the structure was constructed to exhibit a maximal absorption at around [8].

$$f_0 = \frac{c}{2\pi} \sqrt{\frac{\rho_0}{m_s(d_p + d_a)}} \approx 121 \text{ Hz.} \tag{39}$$

To obtain a more precise a priori prediction of the absorption characteristics of the absorber, the layered structure was modeled using the 1-dimensional transfer matrix method (TMM) as described in [3]. The prediction results are shown in Figure 2 (b), taking into account the finite size of the absorber by using a simple radiation efficiency-based correction term while assuming a layered structure of infinite extension.
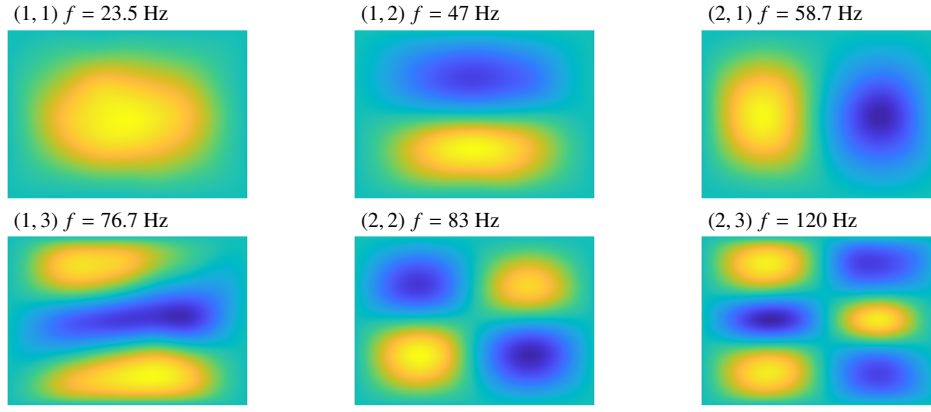
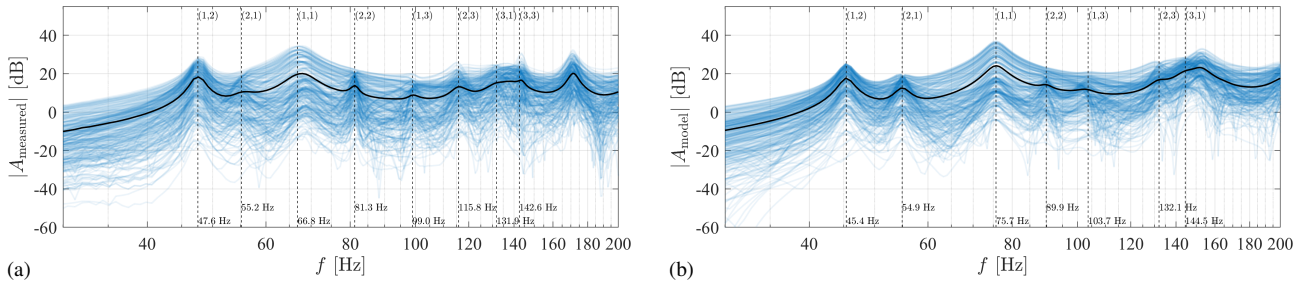Figure 3: Mode shapes and eigenfrequencies measured on the unbaffled, simply-supported top-plate

Figure 4: Measured (a) and modeled (b) plate accelertion with blue line denoting the acceleration of all measurement points and black line denoting the mean of the absolute accelertion vectors

3.2. Defining the propagation speed in the top plate

To estimate the speed of bending waves in the top thin plate, experimental modal analysis was conducted on a disassembled structure with the plate still attached to the framing, allowing both sides to radiate into the free field. The arrangement approximated a simply-supported, unbaffled plate. The first six modes and their eigenfrequencies were analyzed as depicted in Figure 3, and the highly ortotropic nature of the plate with higher wave speed in the x-direction was observed. The modal frequencies were assumed to approximate in-vacuo eigenfrequencies described by Equation 37. However, it should be noted that the actual in-vacou eigenfrequencies are slightly higher then the measured values, since the additional mass of air, moving around the free-standing plate as an acoustic short-circuit, decrease the modal frequencies. This effect is enhanced in case of odd modes with high radiation efficiency.

The lateral wave propagation speed in the plate was estimated to be c_x = 5800 m/s and c_y = 1800 m/s, and slightly increased based on the above physical considerations, for best fit with the analytical 3D model. Additionally, Rayleigh damping was introduced by adding an imaginary part to the propagation speed components, chosen to achieve the best fit with the experimental model. Precise measurement of plate parameters was not within the scope of this study.

3.3. Comparison of analytical model with measurements

In order to compare the modeled resonator with the actual structure, the modal behavior of the top plate backed by the air gap and the porous layer, was investigated. The modal analysis was performed on the plate's normal acceleration. For the analytical model the plate accelartion is calculated from the surface admittance as

$$\mathbf{A} = \frac{1}{dS} \left(\mathbf{I} - 2\rho_0 \mathbf{Y}\mathbf{G}\right)^{-1} \mathbf{Y} \tag{40}$$
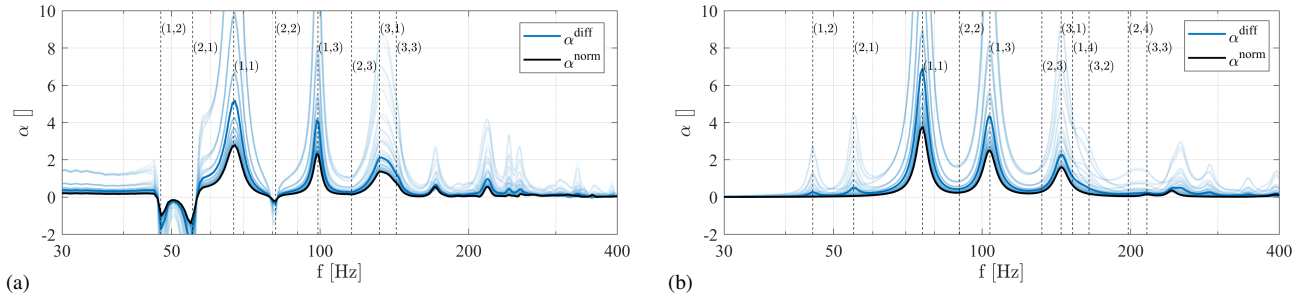
Figure 5: Measured (a) and modeled (b) absorption coefficients of the plate resonator. Transparent blue lines denote the absorbtion coefficient into different directions. Solid blue line denotes the diffuse absorption coefficient and solid black line denotes the normal incidence absorption.

For the actual plate resonator structure the surface acceleration was measured over a grid by exciting the surface with a PCB 086C03 impact hammer and measuring the response with PCB 353B13 accelerometers. The measurement results were interpolated to the grid of the analytical calculations.

The acceleration distribution of the measured and analytical model data is shown in Figure 4 (a) and (b), respectively, with the mean acceleration indicated by the black line. The vertical dashed lines in both graphs represent the identified modes from the modal analysis. Although the low-order eigenfrequencies and corresponding damping are qualitatively estimated correctly, significant errors occur for higher modes. This is likely due to the fact that the plate parameters were estimated based on low-frequency modes, but a more precise estimation of material properties is beyond the scope of this study.

More importantly, the analytical model provides a qualitatively correct approximation of the physical process inside the plate absorber, showing that the order of plate modes strongly depends on the cavity behind the top plate. The mode shapes are categorized based on the number of positive and negative partitions along the surface. Even modes have the same number of positive and negative cells, while odd modes have different numbers of positive and negative cells. Due to the acoustic short circuit above the plate, even modes have low radiation efficiency, while odd modes radiate waves to the upper half-space with low efficiency. Similarly behind the plate, for even modes the pressure fluctuation is locally equalized below the enclosure, and the acoustic short circuit behaves as a concentrated mass connected to the back of the plate, slightly decreasing the in-vacuo modal frequencies. However, for odd modes, the air inside the enclosure must be compressed by the plate, and the cavity acts as an additional stiffness to the plate, resulting in a significant increase in the natural frequency of odd modes (e.g. (1,1)), even above higher-order modes.

3.4. Absorption characteristics of the plate resonator

Finally, the absorption characteristics of the plate resonator were estimated based on the analytical model and was compared with measurement results. For both the analytical model and the measurement based estimation was performed by evaluating Equation 18 and Equation 20 for the normal and diffuse absorption parameters. For the measurement based estimation the admittance matrix was captured by means of impact testing of the top plate on a full grid, with the methodology detailed in [9].

The normal incident, oblique incident and the diffuse absorption factors are illustrated in Figure 5. Comparison with Figure 2 (b) highlights that instead of the ideal absorption factor of the simple mass-spring system the absorption characteristics of the system is mainly determined by the modal behaviour of the top plate. Both the measured results and the analytical model verifies that significant absorption is achieved on odd modes with high radiation efficiency, at which the plate compresses the air inside the cavity (including the porous absorber) due to its motion. At even modes with low

radiation efficieny, the air inside the cavity acts as an acoustic short-circuit, therefore, fluid motion barely reaches the absorber layer. As a result, only minor absorption is achieved at these modal frequencies, enhanced for lateral waves exciting the even modes asymmetrically. It is noted that for the measurement results at low order even modes negative absorption is estimated, which may be the result of phase uncertainty in the measurement result.

In both cases, along with the size-corrected TTM result (see Figure 2 (b)) absorption coefficients above unitiy are predicted. This phenomena is even enhanced for lateral incident waves, with the incident pressure wave generating large plate vibrations at low incident intensities. This apparent unphysical absorption factor exceeding unity reflects that on the plate's modal frequencies the absorber "draws in" energy from surrounding regions due to a process of diffraction, therefore, the actual absorption area highly exceeds the plate's physical dimensions [10].

4. CONCLUSIONS

The present contribution discussed 3D modeling method of finite-sized layered acoustic absorber structures. The study was focusing on rectangular, rigidly baffled absorber geometries consisting of thin plates, air gaps and porous layers, the latter modeled as equivalent fluids. However, the theory can be straightforwardly extended for arbitrary shapes with arbitrary lateral boundary conditions as long a suitable set of modes can be found for the geometry.

The theoretical results were validated via comparison with an actual plate absorber of relatively small size. The comparison showed that the proposed model can predict the absorption characteristics of layered structures qualitatively correctly. However, to achieve a closer match with measurement results, more precise material parameter estimation of the involved layers would be necessary, which is out of the scope of this paper.

Furthermore, the extension of the proposed method for more general structures would require the analytical investigation of slotted, perforated and microperforated plates, which is the subject of further research. Overall, this study provides a useful basis for modeling and predicting the absorption properties of layered acoustic absorber structures, which have important applications in noise control and acoustic design.

REFERENCES

1. P. M. Morse and K. U. Ingard. *Theoretical Acoustics*. McGraw-Hill Book Company, New York, NY, 1st edition, 1968.

2. E. G. Williams. *Fourier Acoustics: Sound Radiation and Nearfield Acoustical Holography*. Academic Press, London, 1st edition, 1999.

3. Jean Allard and Noureddine Atalla. *Propagation of Sound in Porous Media: Modelling Sound Absorbing Materials*. Wiley, 2009.

4. M. E. Delany and E. N. Bazley. Acoustical properties of fibrous absorbent materials. *Applied Acoustics*, 3, 1970.

5. Y. Miki. Acoustical properties of porous materials-modification of delany-bazley models-. *J. Acoust. Soc. Jpn.*, 11(1), 1990.

6. F. P. Mechel. *Formulas of Acoustics*. Springer, 2002.

7. J. F. Allard and Y. Champoux. New empirical equations for sound propagation in rigid frame fibrous materials. *J. Acoust. Soc. Am.*, 91(6), 1992.

8. Trevor Cox and Peter D'Antonio. *Acoustic Absorbers and Diffusers: Theory, Design and Application*. CRC Press, 2016.

9. G. Firtha and Cs. Huszty. Measurement based absorption characteristics estimation of extended reactive surfaces. In *Proceedings of Forum Acusticum 2023*, 2023. Under revision.

10. F. J. Fahy. *Sound Intensity*. Spon Press, 2nd edition edition.